Remote cooling systems with mesh-based heat exchangers for cryogenic applications

A Onufrena[1, 2, 3,*], B Naydenov[1], T Koettig[1], J Bremer[1], T Tirolien[2] and H J M ter Brake[3]

[1] CERN, Technology Department, Cryogenics Group, 1211 Geneva 23, Switzerland
[2] European Space Agency, ESA, 2200 AG Noordwijk, The Netherlands
[3] University of Twente, 7500 AE Enschede, The Netherlands

[*] Corresponding author: aleksandra.onufrena@cern.ch

Abstract. In the refrigeration technologies available for the 2 W - 5 W cooling power range at 4.5 K, innovative designs for intermediate cooling options are proposed between the large-scale cryogenic plants and small-scale commercially available cryocoolers. This paper presents a number of remote cooling solutions, which use high-effectiveness mesh-based counterflow heat exchangers (CFHEX) to support the aforementioned refrigeration domain. Additionally, the cooling power is aimed to be provided in a remote, distributed and non-disturbing manner (i.e. reduced mechanical vibrations and magnetic disturbances) for high-technology cryogenic applications that require very low background noise levels. The proposed remote cooling options are analysed in terms of their cooling power performance. Designs and sizing of individual system components, i.e. CFHEXs and cooling interface options, for superconducting radio frequency (SRF) cavity cooling application are also proposed. CFHEX compactness and influence of their individual effectiveness values on the performance of the remote cooling systems are assessed, and capillary cooling interface performance is analysed.

1. Introduction

A number of high-end technology applications require the refrigeration capacity of several Watts at 4.5 K. These include cooling of superconducting radio-frequency (SRF) cavities in particle accelerators [1] and high-temperature superconductors (HTS) for a range of emerging applications [2]. The state-of-the-art cryocoolers can partially cover the existing cooling needs, but the number of required cryocoolers may be high [3]. Moreover, small cryogenic plants experience a significant drop in their efficiency below 100 W at 4.5 K [2]. This created a motivation to search for alternative cooling solutions.

In addition to the growing need for increased cooling capacity, other challenges are encountered in the attempt to provide cooling for a range of applications. As an example, ultra-sensitive detectors, such as infrared sensors for space missions, cryogenic mirrors of gravitational wave detectors [4] or Superconducting QUantum Interference Device (SQUID) magnetometers in CERN's antiproton decelerator [5] are highly influenced by mechanical vibrations and other disturbances (e.g. temperature and magnetic field variations) that are transported to them from the chosen cooling source. Several approaches have been considered to minimize the transported disturbances, mainly by decoupling the cooling source from the detectors mechanically or by distance. These include using the cryocooler cooling source in combination with flexible conducting straps or heat pipes. However, it is rather difficult to ensure a homogeneous temperature distribution across the cooled object, and to transfer heat

effectively due to heat in-leaks. A well-distributed heat extraction over a large area is also important for cooling of the liquid propellant tanks in the space launchers [6]. As a solution, zero-boil-off (ZBO) arrangements can be considered, where the cooled object is placed directly in the liquid cryogen bath [5]. However, the operation of ZBO cryostats is complex and entails a number of safety concerns.

All this suggests that there is a need for novel systems that provide cooling in a minimized-disturbance, remote, distributed and "dry" (as opposed to cryogen bath) manner as well as increase the cooling power of existing cryocoolers. One promising solution to meet these goals is remote cooling [7-9]. Remote cooling systems consist of a cryocooler and an independent convection loop via which the cooled object is decoupled from the cryocooler mechanically and by distance. Such solutions allow to increase the available cooling power of the cryocooler and to extract heat over larger areas. Additionally, remote cooling systems are compact and inherently flexible, which facilitates their integration into existing installations. Since the amount of fluid in such systems is smaller than that in the ZBO cryostats, the size of the safety devices and, hence, the potential leaks into the cryostat are reduced.

This paper presents a number of remote cooling arrangements that can be used to support the 2 W - 5 W at 4.5 K refrigeration domain, to minimize the transported vibrations and to distribute the cooling effectively across the cooled object. The presented solutions are analyzed in terms of their cooling power for a sample application of SRF cavities. Design, sizing and performance analysis of critical system components i.e. counter-flow heat exchangers (CFHEXs) and capillary cooling interfaces are proposed.

2. Overview of cooling arrangements

Cooling of Nb-coated copper SRF cavities is a challenging real-life application, which is chosen as an example to demonstrate the potential of remote cooling systems to reduce transported vibrations, to decouple the cooling source from the cavity, to reduce the complexity of the cryostat and to further enhance the initial cooling power provided by a cryocooler cooling source.

Several arrangements to cool down an SRF cavity well below its critical temperature are shown in figure 1. In figure 1a, the high-pressure (HP) helium gas is extracted from the compressor of a cryocooler and is passed through a series of pre-cooling stage heat exchangers (HEX) before arriving at the cavity, which is located in a remote cryostat. The proposed cooling interface (CIF) between the pre-cooled fluid and the cavity can be accomplished via a helically wound thin capillary tube that is brazed or chemically etched onto the outer shell of the cavity. Once the fluid exits the CIF, it is used to pre-cool the incoming flow and is then returned to the compressor after passing via a restriction to match the pressure of the compressor's low-pressure (LP) line. The returning flow can also be used to cool down the thermal radiation shield. High pressure of the fluid allows for the designs that comprise small-diameter pipelines of the convection loop with low pressure losses, which leads to reduced vibrations at the CIF [7].

In the arrangement in figure 1b, a separate pump is added to circulate the helium in the system. Moreover, a Joule-Thomson (JT) valve is placed at an appropriate location to further decrease the temperature of the fluid due to JT cooling effect. This configuration enhances the total available cooling power compared to the cryocooler alone, whereas the JT expansion into the two-phase region allows for the CIF to remain at a stable temperature. Since the JT expansion may disturb the fluid stream, it should be ensured that the level of introduced vibrations is sufficiently low for the application in question. A capillary CIF can also be replaced by a bath filled with a saturated liquid helium where the cooled object would be placed. Such a configuration can be of interest for the cooling of a Nb-shield of cryogenic current comparators, where temperature stability and homogeneity are of the key importance [5]. The remote cooling operation in both arrangements requires well insulated transfer lines.

In large-scale applications, such as the Large Hadron Collider (LHC), the SRF cavities are installed horizontally and are cooled in a saturated helium bath at 4.5 K and 1.3 bar supplied by a cryoplant via a JT expansion from a transfer line at 3 bar. During the cooldown of the cryo-module, the level of helium in the bath, which surrounds the cavity, increases. This causes the superconducting front to move gradually through the cavity parallel to the beam axis and may result in a trapped magnetic field. This has a detrimental effect on the performance of the cavity. The cooling arrangements from figures 1c and

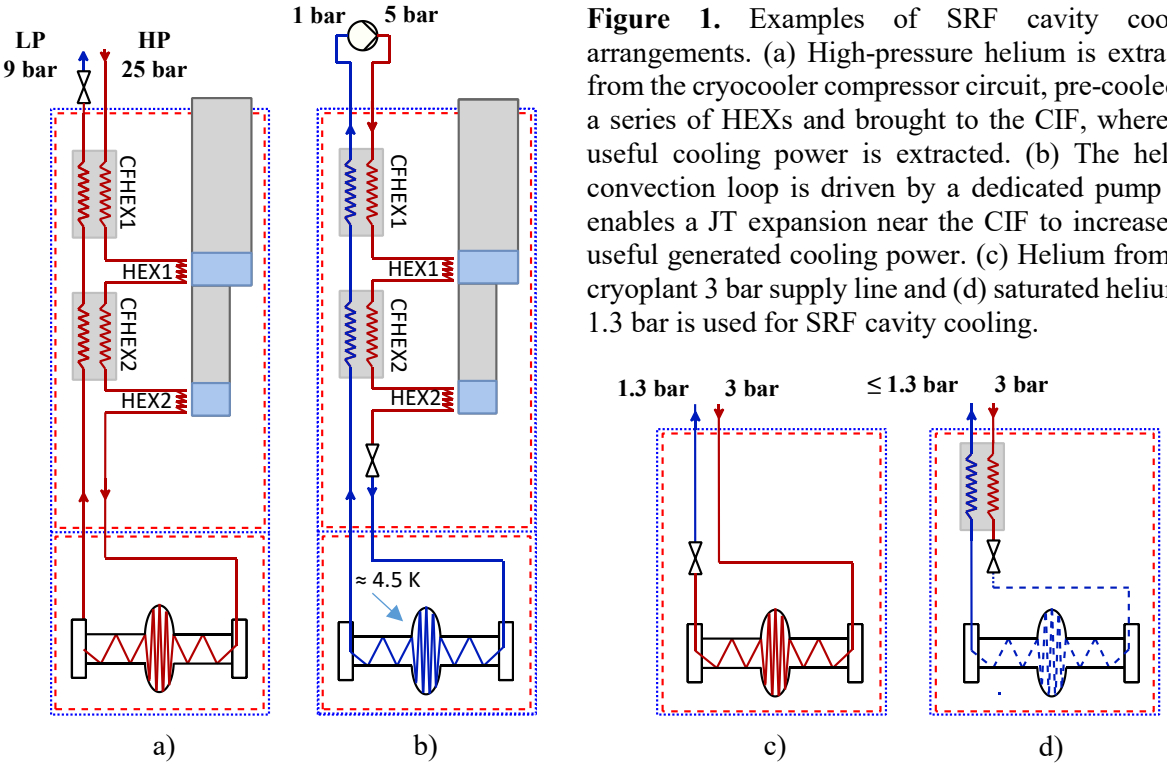

Figure 1. Examples of SRF cavity cooling arrangements. (a) High-pressure helium is extracted from the cryocooler compressor circuit, pre-cooled by a series of HEXs and brought to the CIF, where the useful cooling power is extracted. (b) The helium convection loop is driven by a dedicated pump and enables a JT expansion near the CIF to increase the useful generated cooling power. (c) Helium from the cryoplant 3 bar supply line and (d) saturated helium at 1.3 bar is used for SRF cavity cooling.

1d are proposed to address this issue with SRF cavity cooling for the future applications, such as the Future Circular Collider [10]. In the arrangement in figure 1c, helium at 3 bar and 4.5 K is supplied to the CIF capillary of the cavity that provides the cooling as opposed to a liquid helium bath. This allows the cavity to become superconducting in a controlled manner, which reduces the possibility of the trapped magnetic field. Moreover, supercritical helium at 3 bar in the CIF has a low pressure drop and its behavior is predictable due to the absence of two-phase flow effects. The helium exiting the capillary is then expanded via a JT-valve to 1.3 bar pressure of the return line.

Alternatively, the arrangement in figure 1d can be used if homogeneous temperature distribution around the cavity is sought. In this case, the JT-valve is placed upstream of the cavity, hence the fluid flow that enters the CIF capillary is in a saturated two-phase condition. Its temperature (around 4.5 K) will remain approximately constant until the fluid in the capillary has fully evaporated. Additionally, further pumping of the return line allows bringing helium in the CIF to the superfluid condition, which results in a more effective cooling and a better performance of the cavity at lower temperatures.

2.1. Performance of the remote cooling arrangements

For the systems in figure 1a and 1b, the cooling power depends on the characteristics of the chosen cryocooler (a typical experimentally measured performance map is shown in figure 2), the effectiveness and pressure drop of the CFHEXs and the CIF capillary as well as the operating conditions of the system. The methods to determine the latter are outlined in [8]. In this preliminary study the transfer lines are assumed to be perfectly insulated and have a negligible pressure drop. Depending on the remote system application, their losses should be further analysed in the detailed system design.

In the system in figure 1a, the pressure of the fluid streams matches that of the HP line of the cryocooler's compressor. Under the fixed pressure, it is the helium mass flow rate that will mostly determine the performance of the system. The variation of the CIF temperature, T_{CIF} with the mass flow rate, $\dot{m}$ for a given useful cooling power, $\dot{Q}_{cooling}$ extracted at the CIF is shown in figure 3. It can be seen that a higher deposited heat at the CIF results in a higher T_{CIF} with an optimum $\dot{m}$ for each $\dot{Q}_{cooling}$ line that allows to achieve the lowest T_{CIF}. This can be explained as follows: as $\dot{m}$ increases, the heat is

extracted from the CIF more effectively, hence a lower T_{CIF} is achieved. However, a higher $\dot{m}$ also imposes a greater heat load at the cryocooler stages, leading to a higher stage and CIF temperatures. Due to these two opposing effects, there is an optimum $\dot{m}$ for each given cooling power that allows to achieve the lowest T_{CIF}. Overall, the system in figure 1a achieves similar cooling power at the CIF as the cryocooler alone (i.e. 2 W at 4.5 K), but at higher CIF temperatures. However, this cooling configuration can be particularly interesting for the applications that aim to reduce the transported vibrations and target a low cooling power, e.g. superconducting Nb-shield in [5] requires ≈ 1 W of cooling below 9.3 K.To further optimize the system in figure 1a, the designer may consider moving the JT-valve to the outlet of the 2nd stage HEX where an additional cooling effect can be achieved. If the fluid is expanded to a typical pressure of the compressor's LP line of 9 bar, the maximum cooling is achieved at around 10 K. Alternatively, an isentropic expansion can provide an even greater cooling effect.

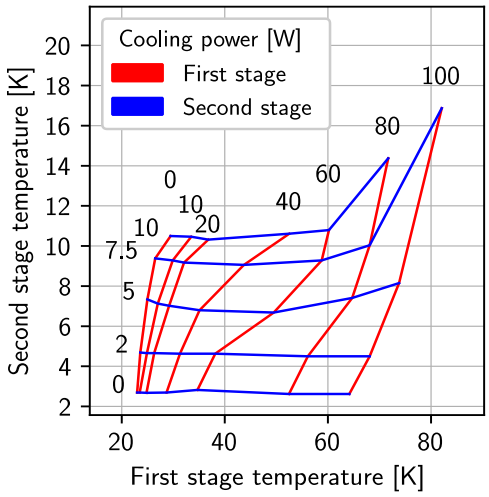

Figure 2. Cooling power of a two-stage cryocooler for a range of 1st and 2nd stage temperatures experimentally measured at the CERN Cryolab. The maximum temperature and power measurement uncertainties are ±0.1 K and ±0.1 W, respectively.

The system in figure 1b aims to maximize the cooling power by means of a JT expansion. In this case, the temperature of the saturated helium in the CIF is determined by the outlet pressure of the JT valve. The latter amounts to 1.3 bar, which results in the CIF temperature of 4.5 K (for the outlet pressure of the system of 1 bar and the combined CFHEX pressure drop of 300 mbar). The optimum inlet pressure of the JT valve was found to be ≈ 5 bar at 6 K (see previous studies for details [8]). For such system, $\dot{Q}_{cooling}$ at 4.5 K primarily depends on, and increases with, $\dot{m}$ as seen in figure 4. It can also be seen that $\dot{Q}_{cooling}$ is vastly affected by the CFHEX effectiveness, which is further discussed in section 2.2.1. This arrangement from figure 1b can almost double the cooling power at 4.5 K as opposed to using the cryocooler alone.

2.2. Critical component design

The maximum cooling power achieved by a remote cooling system is driven by the design and performance of its critical components, i.e. CFHEXs and the CIF capillary, which are outlined and analysed in this section.

2.2.1. CFHEXs. As it is evident from figure 4, the effectiveness of the CFHEXs has a strong effect on the system's performance at high mass flow rates. By increasing the effectiveness from 93 % to 98 %, the cooling power at 4.5 K can be increased from 2.8 W to 3.6 W for $\dot{m} = 200$ mg/s, whereas only 2 W at 4.5 K is available with the chosen cryocooler alone. CFHEXs of such high effectiveness are often significant in size [7]. Mesh-based CFHEXs have a great potential to provide a high-effectiveness compact design, which will allow implementation of the remote cooling systems in the new and existing installations [8, 9, 11]. The calculations show that a

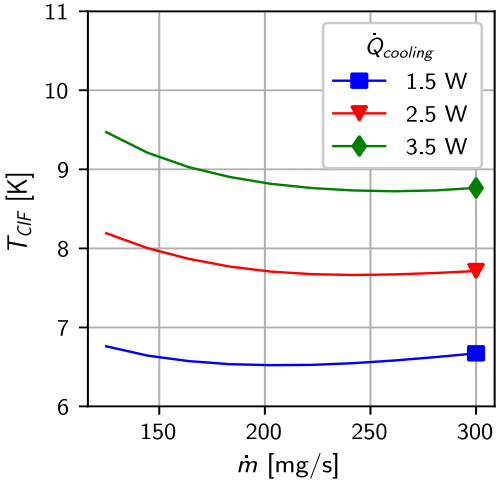

Figure 3. Variation of the CIF temperature with the mass flow rate for a given extracted cooling power for the system from figure 1a. CFHEX effectiveness of 96 % and pressure drop of 100 mbar per CFHEX stream are assumed. Cryocooler data, see figure 2.

factor of 10 reduction in volume when compared with a classic concentric tube-in-tube CFHEX can be achieved. In the standard configuration, a mesh-based CFHEX consists of two concentric tubes filled with layers of woven mesh screens that act as fins to enhance the heat transfer between the flows. CFHEX effectiveness depends strongly on conductance of the contact between the mesh and the inner tube, and the axial conduction along the CFHEX [8]. If the mesh-to-inner tube contact conductance is increased while the low axial conductance is maintained, an even more effective and, hence, more compact design can be constructed. The increase in the contact conductance can be accomplished by soldering the mesh to the inner wall or applying sophisticated additive manufacturing techniques [9].

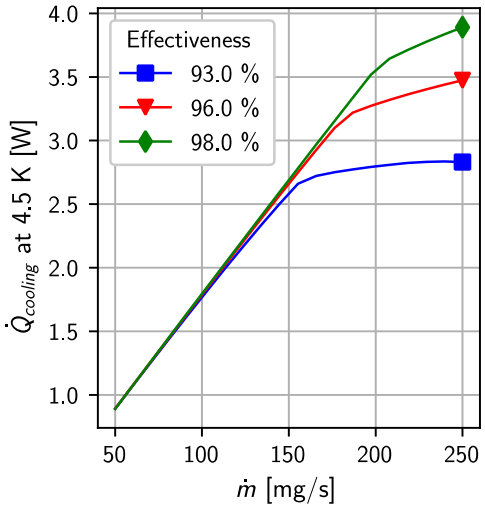

Figure 4. Variation of the cooling power at 4.5 K CIF vs. mass flow rate for different CFHEX effectiveness for the system from figure 1b. Pressure drop of 100 mbar per CFHEX stream are assumed.

2.2.2. Cooling interface. A CIF that is used to extract the heat from the cooled object can be accomplished in a number of ways depending on the application. In our example of the SRF cavity cooling, the proposed design consists of a thin helically wound capillary tube, which is brazed or chemically etched onto the outer shell of the cavity to ensure a well-distributed heat extraction over its surface (see figure 1).

There is a wide field of parameters that affect the performance of the capillary CIF in terms of its heat transfer capabilities and pressure drop. These include diameter and length of the capillary, the fluid flow phase, vapor quality (for a two-phase flow), operating conditions of the system and the heat deposited on it. The following approach was taken to determine an optimum CIF design for the SRF cavity cooling: operating conditions of the used cooling arrangement were identified, the baseline CIF geometry was defined, and then individual geometry parameters were varied to analyze their influence on the performance of the CIF. The baseline geometry and nominal operating conditions are:

- Mass flow rate ($\dot{m}$): 200 mg/s of helium (based on optimum values from figures 3 and 4).
- Typical fluid temperature at the CIF capillary inlet ($T_{CIF,in}$): 4.5 K.
- Baseline capillary geometry: length of 10 m, inner diameter of 3 mm, wall thickness of 0.5 mm.
- Typical heat-load: 3 W (homogeneously distributed along the capillary CIF).

For the cooling arrangements in figure 1, the flow in the CIF can be under various pressure conditions, which are summarized in table 1.

Table 1. Pressure and flow conditions in the capillary CIF.

Cooling arrangement	**Nominal pressure and flow type in the CIF**
System from figure 1a at high-pressure	Pressure: 25 bar or 9 bar (depending on the position of JT valve). Flow type: supercritical single-phase flow.
System from figure 1b with JT enhanced cooling	Pressure: 1.3 bar. Flow type: saturated helium, two-phase flow (TPF).
Cavity cooling using the supply lines of an LHC-like cryoplant from figure 1c and 1d.	Pressure: 1.3 bar or 3 bar (based on the position of JT-valve). Flow type: saturated or supercritical flow near the pseudocritical line.

For all these conditions, temperature and pressure drop performance of the CIF was analyzed. Figure 5a shows the evolution of the fluid temperature along the CIF for the baseline geometry. The temperature of the single-phase flow (3 bar - 25 bar cases) increases along the capillary as the heat is absorbed. For the two-phase flow (TPF) case, very small temperature differences along the capillary are expected.

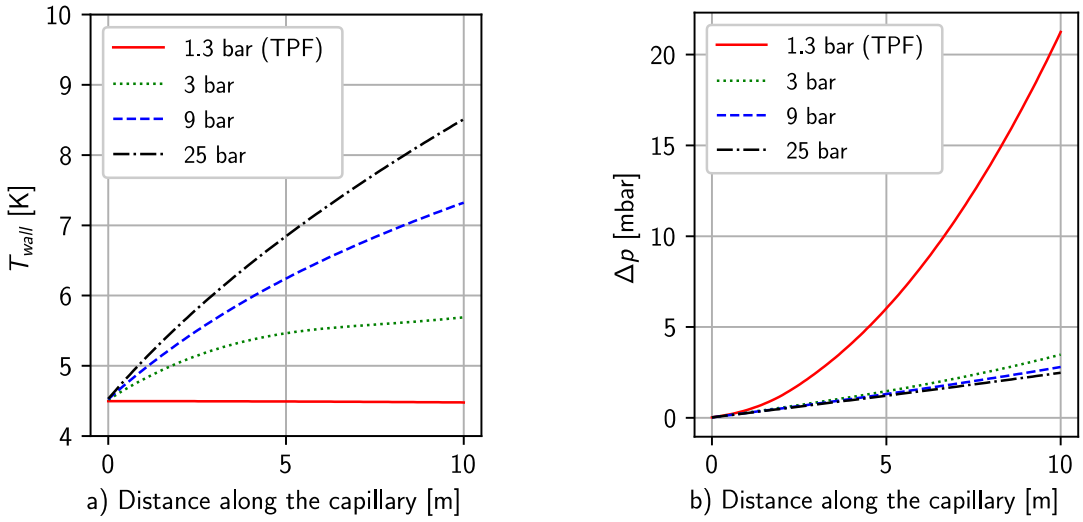

Figure 5. (a) Fluid temperature and (b) pressure drop variation along the capillary CIF for various flow conditions. CIF inner diameter is 3 mm, heat load is 3 W (distributed), $\dot{m} = 200$ mg/s, $T_{CIF,in} = 4.5$ K.

Moreover, as the pressure along the capillary decreases, a slight progressive decrease of the saturation temperature of the TPF can be observed in figure 5a. It can be seen from figure 5b that the pressure drop is larger for the TPF and similar among the three single-phase flow cases. Among the single-phase flow cases, the lowest CIF temperature is achieved for the flow at 3 bar. This is due to the operating temperature and pressure conditions laying near the pseudocritical line in the supercritical region, where the heat transfer coefficient is higher than that of a "gas" flow. As a result, 3 bar flow can be a promising candidate for certain applications, combining high heat transfer and the absence of TPF effects.

Figure 6a shows the variation of the average temperature difference, ΔT between the flow and the capillary wall, which represents the heat transfer capabilities, with the capillary's diameter for different flow conditions. It can be seen that the ΔT at the wall-to-fluid interface is lower for smaller diameters, thus the heat transfer is more effective. However, the pressure drop is higher for smaller diameters as evident from figure 6b. The lowest ΔT is achieved in the TPF regime, where the heat transfer coefficient is the highest. However, for smaller diameters, the fluid near-the-pseudocritical line at 3 bar has a similar thermal performance while offering a smaller pressure drop. For all single-phase flow cases (3 bar - 25 bar) the pressure drop is almost the same. Figure 7 shows the variation of the ΔT at the wall-to-fluid

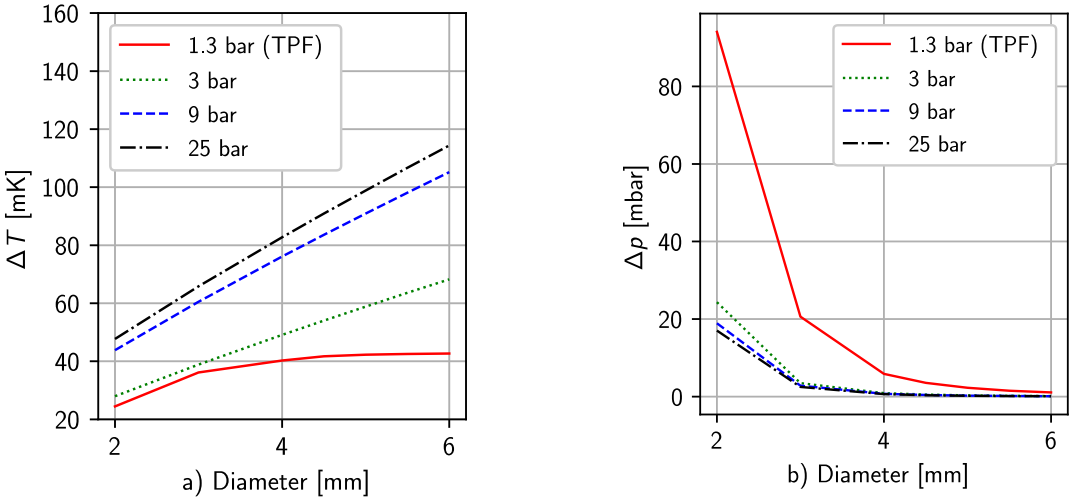

Figure 6. Influence of the capillary's diameter on (a) the difference between the average capillary and fluid temperatures, and (b) the total pressure drop for different flow conditions. CIF length is 10 m, heat load is 3 W (distributed), $\dot{m} = 200$ mg/s, $T_{CIF,in} = 4.5$ K.

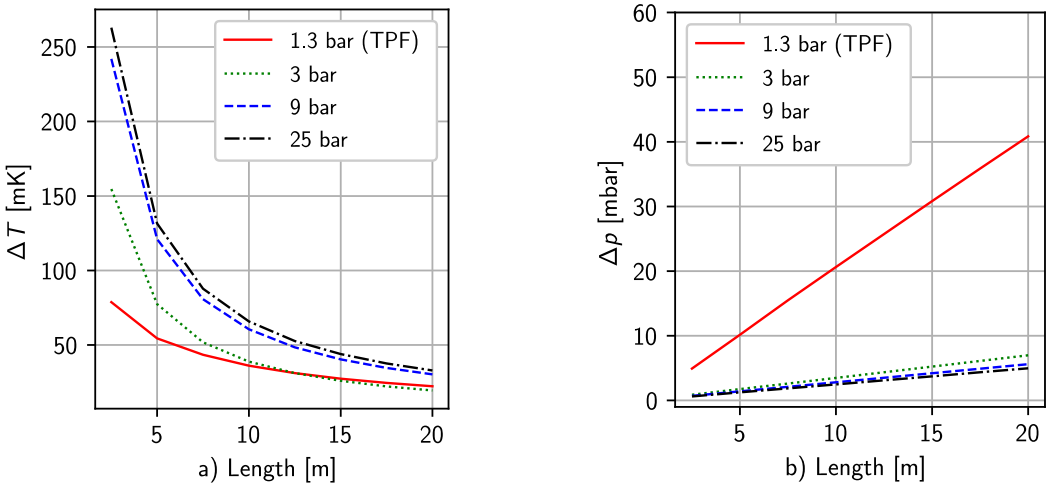

Figure 7. (a) The difference between the average capillary and fluid temperatures, and (b) accumulated pressure drop as a function of total capillary length for different flow conditions. CIF inner diameter is 3 mm, heat load is 3 W (distributed), $\dot{m} = 200$ mg/s, $T_{CIF,in} = 4.5$ K.

interface and the pressure drop with the length of the capillary. For all flow conditions, a longer CIF results in lower a ΔT and a greater pressure drop. The heat transfer is the highest in the TPF case. The decrease in ΔT slows down above 10 m for all case, thus this value was chosen as a baseline CIF length.

As seen from figures 5, 6 and 7, the TPF is an interesting design choice due to its high heat transfer capabilities. However, an elaborate modelling is required to analyse it as the heat transfer coefficient in the TPF strongly depends on the flow regime. The latter is a function of the vapour fraction and total mass flux that form a flow pattern map as shown in figure 8. The location of the areas denoting specific flow regimes (marked on the map) depends on a set of flow and geometric parameters. Thus, an individual map has to be created for each given system and its operating conditions. In figure 8, the blue dashed line represents the flow evolution in the CIF. The fluid enters the capillary as a saturated liquid and its vapour quality increases as it evaporates. It is highly desired that the dry-out regime is not reached in the capillary during the operation to avoid the deterioration of the heat transfer and, thus, the temperature rise of the cavity.

The temperature distribution of the cavity depends on the number of CIF capillary loops around its outer shell. A proposed placement of these loops and a typical profile of the heat load by RF losses are shown in figures 9a and 9b. For such geometry, a temperature profile of the cavity was determined using a one-dimensional numerical model and is shown in figure 9c for various flow conditions. The temperature gradients between the capillary loops were found to be below 1 mK for all cases. The temperature of the cavity increases progressively for all single-phase flow cases as the flow in the CIF warms up. In the TPF case, the flow is at an almost constant temperature and its distribution is homogeneous.

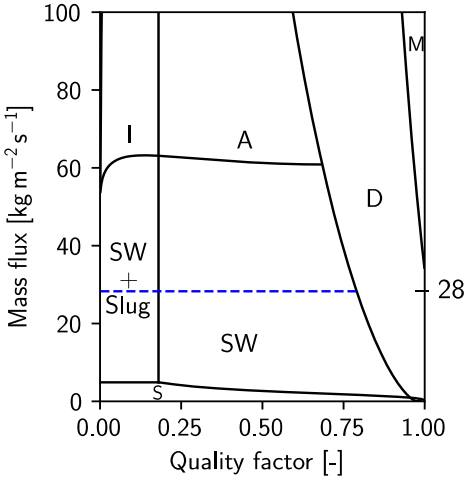

Figure 8. The pattern map for TPF helium inside the CIF (method from [12]). The solid lines separate the areas of the denoted TPF regime: **I**ntermittent, **A**nnular, **D**ryout, **M**ist, **S**tratified, **S**tratified-**W**avy, Slug. The dashed line indicates the flow in the CIF with the baseline geometry at $\dot{m} = 200$ mg/s (i.e. 28.3 kg/m^2/s).

3. Conclusions

For several high-technology applications, a distributed and reduced-disturbance cooling is required. With that purpose, two cryocooler-based remote cooling systems are proposed and analysed in terms of their performance. The high-pressure

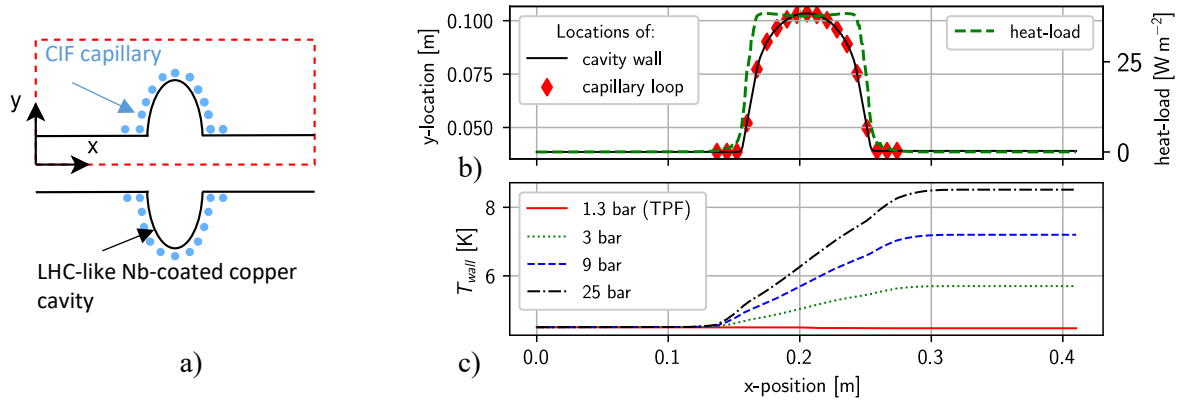

Figure 9. (a) Schematic of an SRF cavity with the CIF capillary. (b) Typical heat load in the cavity (total heat-load: 3 W) and the *y*-location of the capillary loops as a function of *x* positions as per (a). (c) The temperature profile along the cavity for different flow conditions.

loop is shown to have a lower pressure loss and is expected to reduce vibrations at the CIF, while the JT expansion-based circuit allows to increase the cryocooler's cooling power from 2 W to 3.6 W at 4.5 K.

Distributed cooling of the SRF cavities was chosen as a challenging real-life application for the remote cooling systems. For this application, the designs of the critical system components (CFHEXs and CIF capillary) are proposed and their behaviour is analysed. Mesh-based CFHEXs are suggested to satisfy high effectiveness and compactness requirements. The CIF capillary is sized and the effects of various geometry parameters and flow conditions on its behaviour are analysed. It is found that TPF in the CIF has the largest heat transfer potential and allows achieving a constant temperature ($\Delta T < 1$ mK) around the cavity as long as the dry-out regime is not reached. Alternatively, using a single-phase flow at 3 bar allows for a lower pressure drop than TPF along with a relatively high heat transfer coefficient. The designer can also consider splitting the capillary into parallel channels to reduce the total pressure drop and achieve a more homogeneous temperature distribution for the different flow conditions [6].

Apart from enabling the reduced-vibration cooling of the SRF cavities, remote cooling systems present a strong option for cooling of the parts of the gravitational wave detectors [4].

4. References

[1] *Ciovat G. et al.,"Design of a cw, low-energy, high-power superconducting linac for environmental applications", Phys. Rev. Accel. Beams (2018).*
[2] *Decker L., "Overview on cryogenic refrigeration cycles for large scale HTS applications" (2016).*
[3] *Virostek S., M. A. Green, "The results of tests of the MICE spectrometer solenoids"(2010).*
[4] *Akutsu T., "Large-scale cryogenic gravitational-wave telescope in Japan: KAGRA" (2015).*
[5] *Fernandes M. et al., "Optimized cryogenic current comparator for CERN's low-energy antiproton facilities", Proceedings of IBIC (2016).*
[6] *Plachta D. et al., " Liquid Nitrogen Zero Boiloff Testing", NASA/TP—2017-219389 (2017).*
[7] *Trollier T. et al. "Remote helium cooling loops for laboratory applications",Cryocoolers 17 (2012)*
[8] *Onufrena A. et al., "Design of a compact mesh-based high-effectiveness counterflow heat exchanger", International Journal of Heat and Mass Transfer (2021).*
[9] *Onufrena A. et al., "Cryogenic performance of a compact high-effectiveness mesh counter-flow heat exchanger" (will be submitted to "Cryogenics" in 2021).*
[10] *Abada A., et al., "FCC-ee: The Lepton Collider (Future Circular Collider Conceptual Design Report Volume 2)", Eur. Phys. J. Special Topics 228, 261–623 (2019).*
[11] *Onufrena A. et al., "Characterization of woven copper mesh as a heat transfer matrix at low temperatures", Cryocoolers 21 (2021).*
[12] *Wu J. et al., "Investigation of heat transfer and pressure drop of CO2 two-phase flow in a horizontal minichannel", International Journal of Heat and Mass Transfer (2011).*